

# Disorder and Segregation in B–C–N Graphene-Type Layers and Nanotubes: Tuning the Band Gap

Jonathan da Rocha Martins<sup>†,‡</sup> and Hélio Chacham<sup>‡,\*</sup>

<sup>†</sup>Departamento de Física, Universidade Federal do Piauí, Campus Ministro Petrônio Portela- Bairro Ininga, 64049-550, Teresina, PI, Brazil, and <sup>‡</sup>Departamento de Física, ICEX, Universidade Federal de Minas Gerais, CP 702, 30123-970, Belo Horizonte, MG, Brazil

Boron–carbon–nitrogen (B–C–N) layers and nanotubes have attracted recent interest in the literature<sup>1–10</sup> due to their novel structural, optical, and electronic properties. These materials, first synthesized in the mid-1990s,<sup>11,12</sup> have band gaps and other electronic properties that are intermediate between those of pure carbon and BN.<sup>13–16</sup> Regarding structural properties, recent experimental results on graphene-type B–C–N layers confirm that segregation into either graphene islands in a planar BN matrix<sup>1</sup> or BN islands in a graphene matrix<sup>2</sup> depends on the B–C–N stoichiometry. Regarding optical and electronic properties, it is clear from the available experimental data that the band gaps of B–C–N nanotubes are determined not only by the (x,y,z) stoichiometry but also by other structural properties. For instance, B–C–N nanotubes with  $y \approx 0.1$  (small carbon content) may have band gaps on the order of 2.8 eV,<sup>7</sup> while nanotubes with  $y \approx 0.5$  may have band gaps in the 1.4–2.1 eV range,<sup>17,18</sup> and nanotubes with 1:1:1 stoichiometry may have band gaps on the order of 3.9 eV.<sup>5</sup> These contradict a “mean-field” picture in which the band gap would increase monotonically with decreasing carbon content and suggest that structural properties, such as compositional order/disorder, defects,<sup>7</sup> and chirality, may have important roles in the electronic and optical properties.

From the theoretical point of view, several models have been proposed for B–C–N layers and nanotubes, and their electronic properties have been investigated.<sup>2,19–33</sup> The earliest first-principles model for these materials was proposed by Liu *et al.*<sup>20</sup> They considered an 8 atom unit cell model for a BC<sub>2</sub>N layer and

**ABSTRACT** We investigate structural and electronic properties of B–C–N (boron–carbon–nitrogen) layers and nanotubes considering the positional disorder of the B, C, and N atoms, using a combination of first principles and simulated annealing calculations. During the annealing process, we find that the atoms segregate into isolated, irregularly shaped graphene islands immersed in BN. We also find that the formation of the carbon islands strongly affects the electronic properties of the materials. For instance, in the case of layers and nanotubes with the same number of B and N atoms, we find that the band gap increases during the simulated annealing. This indicates that, for a given stoichiometry, the electronic and optical properties of B–C–N layers and nanotubes can be tuned by growth kinetics. We also find that the excess of B or N atoms results in large variations in the band gap and work function.

**KEYWORDS:** graphene · nanotubes · B–C–N · structural properties · electronic properties · band gap · monolayer hexagonal BN · monolayer h-BNC

obtained a minimum-energy structure with alternating carbon and BN chains which maximized the number of C–C and BN bonds. Miyamoto *et al.*<sup>21</sup> considered that low-energy structure as a basis for BC<sub>2</sub>N nanotubes and obtained interesting properties associated with the chirality of the carbon chains. Blase *et al.*,<sup>22,23</sup> as well as Ci *et al.*,<sup>2</sup> considered BC<sub>2</sub>N structures with alternating ribbon regions of carbon and BN. They showed that the larger the width of the pure ribbons, the lower is the energy, indicating a strong tendency for C/BN segregation. They also found that the band gaps decrease with increasing ribbon widths. Mazzoni *et al.*<sup>19</sup> considered several possible B–C–N stoichiometries (besides BC<sub>2</sub>N) in 8 atom unit cells and obtained a B<sub>3</sub>C<sub>2</sub>N<sub>3</sub> structure with smaller energy than the BC<sub>2</sub>N ones. They also found that the band gaps of the investigated structures are dependent on the stoichiometry and on the specific structure.

In the present work, we investigate theoretically the role of the (B,C,N) positional disorder in the electronic structure of B–C–N nanotubes and graphene-type layers

\*Address correspondence to chacham@fisica.ufmg.br.

Received for review July 28, 2010 and accepted December 10, 2010.

Published online December 27, 2010. 10.1021/nn101809j

© 2011 American Chemical Society

**TABLE 1. Characteristics of the Seven B–C–N Theoretical Samples: Number of C, B, and N Atoms; Eigenvalues  $\epsilon_H$  and  $\epsilon_L$  of the Highest Occupied and of the Lowest Unoccupied Eigenstates, for the Atomic Layer Configurations at the End of the Simulated Annealing Procedure**

sample	C	B	N	$\epsilon_L$ (eV)	$\epsilon_H$ (eV)
a	33	31	32	−3.06	−3.56
b	31	32	33	−3.60	−5.07
c	32	32	32	−3.70	−5.03
d	31	33	32	−4.96	−5.32
e	28	34	34	−3.57	−4.92
f	31	34	31	−5.31	−5.55
g	31	31	34	−3.24	−3.53

employing a combination of *ab initio* and model calculations. First, we apply a bond-energy model,<sup>19</sup> parameterized from first principles, to a simulated annealing process. Then, the electronic structure of selected configurations is investigated from first principles (see Methods section). During the annealing process, we find that the carbon atoms segregate into isolated islands. This is consistent with recent experimental results.<sup>1,2</sup> As the islands are formed, we also find that the electronic density of states evolves from a featureless, gapless  $D(E)$  to one that has a band gap near the Fermi level. This indicates that, for a given stoichiometry, the electronic and optical properties of B–C–N nanotubes and layers can be tuned by the degree of positional disorder.

## RESULTS AND DISCUSSION

As in the case of carbon<sup>34</sup> nanotubes, we will use the  $(n,m)$  indexing to define the nanotube chiral structure.

In carbon nanotubes, the electronic structure is strongly dependent on chirality,<sup>34</sup> while in BN nanotubes, it is not.<sup>35</sup> As models for the B–C–N nanotubes, we will first consider zigzag (6,0) and armchair (4,4) nanotubes, both with a large unit cell of 96 atoms. The diameter of such tubes corresponds to the lower bound in synthesized B–C–N nanotubes.<sup>6</sup> We will also consider graphene-like B–C–N layers, also with large unit cells of 96 atoms. Besides modeling monolayers of hybridized boron nitride and graphene, this would also provide a model for large diameter nanotubes.

In an initial configuration, we randomly select, for each of the 96 sites, that the atom at that site is B, C, or N with equal probability. This corresponds to an intentional 1:1:1 stoichiometry. However, due to the random nature of the procedure, the resulting stoichiometry is slightly off the intentional one. To take into account these local fluctuations in stoichiometry (which should occur in real samples), we consider a small ensemble of “theoretical samples” resulting from the initial sorting procedure, each one with its own stoichiometry. The number of B, C, and N atoms in each of the seven samples is shown in Table 1.

To build the model of B–C–N layers, the cells are periodically repeated along the layer plane, and the geometry is optimized using the first-principles methodology described below. To build the model of B–C–N nanotubes, the cells are deformed into a cylindrical unit cell, which is periodically repeated along the tube axis, and the geometry is further optimized from first principles. As the cells are rectangular-shaped, with borders along either the zigzag or the armchair directions, we can build either zigzag (6,0) or armchair (4,4) nanotubes.

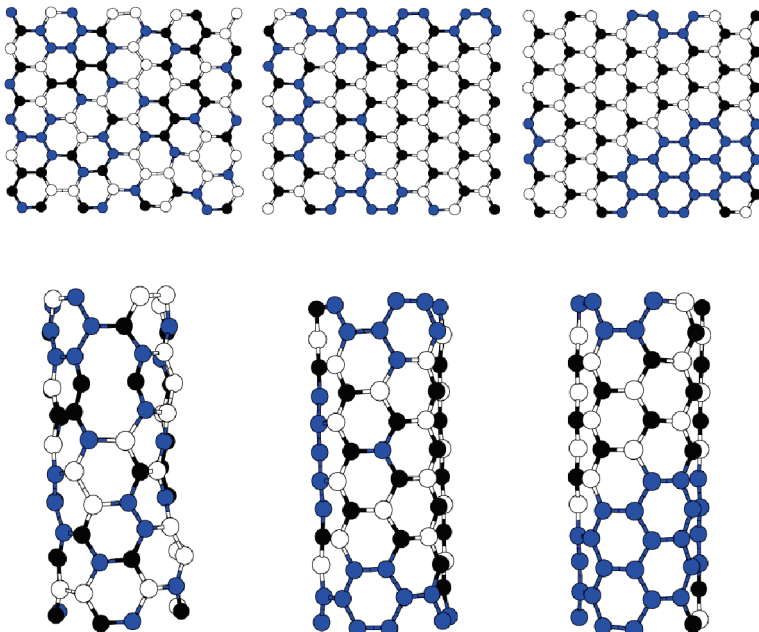


**Figure 1.** Optimized geometries of the unit cells of B–C–N layers (top) and armchair nanotubes (bottom) corresponding to sample c of Table 1. Left: layer and nanotube models corresponding to the initial random configuration of B, C, and N atoms. Middle and right: resulting models during the simulated annealing process, respectively, after  $18 \times 10^6$  and  $38 \times 10^6$  Monte Carlo steps. The blue, black, and white circles represent carbon, boron, and nitrogen atoms, respectively.

In Figure 1, we show the optimized geometries of the unit cells of B–C–N layers (top) and armchair nanotubes (bottom) corresponding to sample c of Table 1, which has 32 atoms of each type. In Figure 2, we show the corresponding geometries for the zigzag nanotubes. In the left panels of Figures 1 and 2, we show the layer and nanotube models corresponding to the initial random configuration of B, C, and N atoms. In the middle and right panels of Figures 1 and 2, we show the resulting models during the simulated annealing process, to be described below.

Having set the initial random configuration of each of the seven samples (either nanotubes or layers), we proceed to a configurational optimization through a Monte Carlo simulated annealing<sup>36</sup> procedure. In this procedure, at iteration  $i$ , we randomly select first-neighbor atoms in the unit cell and exchange these atoms with probability  $P = \min[1, e^{(-\Delta E/k_B T_i)}]$  where  $\Delta E$  is the total energy change upon the atom exchange and  $T_i$  is the simulation temperature at iteration  $i$ .  $\Delta E$  is calculated with a previously proposed bond-energy model<sup>19</sup> (see Methods section). The Monte Carlo simulations aim at obtaining unbiased, low-energy B–C–N structures. For that purpose, the initial temperature was set at  $T_0 = 11\,600$  K, ensuring a complete B, C, N atom-type disorder at the beginning of the simulation. The atomic positions are fixed and are not degrees of freedom in the Monte Carlo simulation; therefore, the fact that  $T_0$  is higher than the fusion temperature of carbon, 3800 K, is not relevant for the purposes of the simulation. The temperature decreases linearly as a function of the number of Monte Carlo iterations, in such a way that at iteration  $i$  the temperature is  $T_i = T_0(\max - i)/\max$ , where  $\max$  is the maximum number of iterations.

In Figure 3, we show several stages of the simulated annealing procedure of sample a, starting from the initial, random configuration of B, C, and N atoms, up to the final, stable configuration after 40 000 000 Monte Carlo steps. The figure shows that, in the early stages of the annealing (up to about 50 000 steps), the atomic exchanges result in the reduction of “wrong” B–B and N–N bonds, leading to a mixture of small carbon and BN regions. After a few million Monte Carlo steps, these small regions start to coalesce, leading to a progressive segregation of B–C–N into separate graphene and “BN graphene” regions. All of the seven samples depicted similar evolutions along the simulated annealing procedure, resulting in irregular graphene islands that tend to form zigzag edges on their borders. In particular, for structures with the same number of B and N atoms, the number of C–N bonds at the border of the graphene island is the same as the number of C–B bonds (this can, in fact, be proven as a theorem). We find that, in all cases, for different initial configurations and stoichiometries, the single-island formation occurs at nearly 80% of the steps, at temperatures on the order of 2300 K. We should mention that

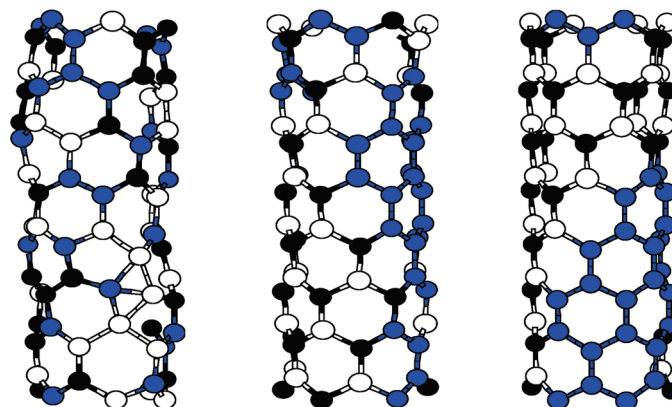


Figure 2. Optimized geometries of the unit cells of B–C–N zigzag nanotubes corresponding to sample c of Table 1. Left: initial random configuration of B, C, and N atoms. Middle and right: configurations after  $18 \times 10^6$  and  $38 \times 10^6$  Monte Carlo steps, respectively. The blue, black, and white circles represent carbon, boron, and nitrogen atoms, respectively.

there is no time scale in the Monte Carlo simulations. Therefore, comparison with experimentally obtained island-formation temperatures is limited because the latter would depend on the cooling rate.

As discussed in the previous paragraph, the Monte Carlo simulations result in irregular-shaped graphene islands. We also considered the possibility of formation of a regular-shaped island. Among the considered theoretical samples (from a to g, see Table 1), sample c has 32 carbon atoms. These atoms can be arranged in a symmetrical shape. We have performed a geometry-optimized first-principles calculation for this regular-island structure, which is shown in Figure 4. The total energy of this structure is 29 meV per carbon atom lower than that of the corresponding irregular-shaped island obtained by the Monte Carlo procedure; therefore, the symmetrical structure is more stable. Interestingly, both types of islands (regular and irregular) have been observed in recent experiments. In the work by Ci *et al.*,<sup>2</sup> all islands have irregular shapes, while in the work by Krivanek *et al.*,<sup>1</sup> a small, symmetrical island of 6 carbon atoms was observed.

We have seen that the main phenomenon that occurs during the simulated annealing is the progressive segregation of B–C–N into larger carbon and BN regions. (The tendency toward segregation is consistent with a previous first-principles study<sup>22</sup> that shows that, in the case of B–C–N layers and nanotubes consisting of alternate stripes of C and BN, the ones with the lowest energy per atom are those with the widest stripes.) Let us now investigate the consequences of this segregation on the electronic properties of B–C–N layers and nanotubes. This will be done by selecting characteristic stages in the simulated annealing process and by performing first-principles calculations with full geometry optimization for those stages. We have chosen three stages: the initial random distribution of B, C, and N atoms; the final, converged structure after the anneal-

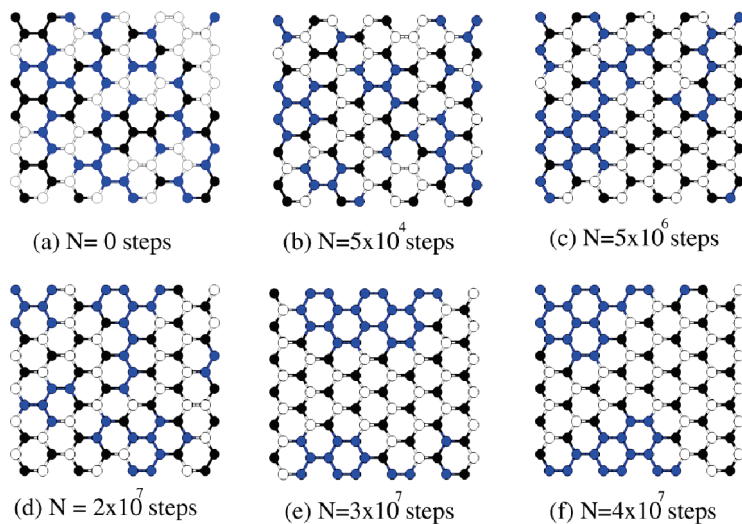


Figure 3. Several stages of the simulated annealing procedure of sample a, starting from the initial, random configuration of B, C, and N atoms, up to the final, stable configuration after 40 000 000 Monte Carlo steps. The blue, black, and white circles represent carbon, boron, and nitrogen atoms, respectively.

ing process; and an intermediate stage, after  $18 \times 10^6$  Monte Carlo steps.

Figure 5 shows the evolution of the total density of states,  $D(E)$  (broadened by Gaussians with a standard deviation of 0.5 eV), of a B–C–N layer built from sample c, which has an equal number of B, C, and N atoms, on the three stages of the simulated annealing process. The position of the B, C, and N atoms in the layer unit cell is shown in the top panel of Figure 1 for the three stages. In the initial stage (random distribution of atoms), the electronic structure of the layer does not present a band gap at  $E_F$ , and  $D(E)$  is essentially featureless. At the intermediate stage (after  $18 \times 10^6$  Monte Carlo steps), a strong depletion of  $D(E)$  in a region of about 1 eV near the Fermi level  $E_F$  can be clearly seen. At the final stage (converged structure), the depletion of  $D(E)$  near  $E_F$  widens and takes the characteristic V shape of  $D(E)$  of graphene near  $E_F$ .

In Figure 6, we show the evolution of the band structure of the (4,4) B–C–N nanotube built from sample c and shown in the lower panel of Figure 1. (One should

note that the band dispersions shown in Figure 5 and 6 should not be taken as dispersions for the real systems, but rather effects of a finite unit cell in a model with periodic boundary conditions simulating a disordered system.) The position of the B, C, and N atoms in the nanotube unit cell is shown in the bottom panel of Figure 1 for the three stages. In the initial stage, the electronic structure of the nanotube does not present a band gap at  $E_F$ , with bands crossing the Fermi level. At the intermediate stage, a band gap of about 1 eV appears in the band structure. In the final stage, a wider band gap of 1.6 eV develops. Interestingly, the lowest unoccupied band for the intermediate stage corresponds to a localized electron state near the isolated carbon atom, surrounded by four nitrogen atoms, that can be seen in the lower-middle panel of Figure 1. At the final stage of the Monte Carlo simulation, this isolated carbon atom is removed from the BN region. To estimate the energy barrier for such a diffusion process, we have performed a geometry-optimized first-principles calculation where we replace the isolated carbon atom with the nitrogen atom at its left in Figure 1. The calculated energy cost for such an atom exchange is 3.8 eV.

The evolution of the electronic structure of the (6,0) B–C–N nanotube during the simulated annealing process is shown in Figure 7. The corresponding nanotube geometries are shown in Figure 2. In the initial, atom-disordered stage, the electronic structure presents a small band gap of 0.21 eV. In the intermediate stage, the band gap increases to 0.48 eV, and in the final stage, it reaches 0.63 eV. Therefore, a similar phenomenology regarding the evolution of the electronic structure (the progressive increase of the band gap) was found for the B–C–N layer, the B–C–N zigzag nanotube, and the B–C–N armchair nanotube.

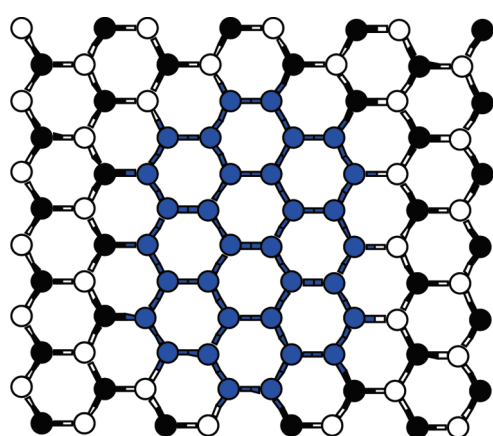


Figure 4. Symmetrical, regular-shaped island of 32 carbon atoms.

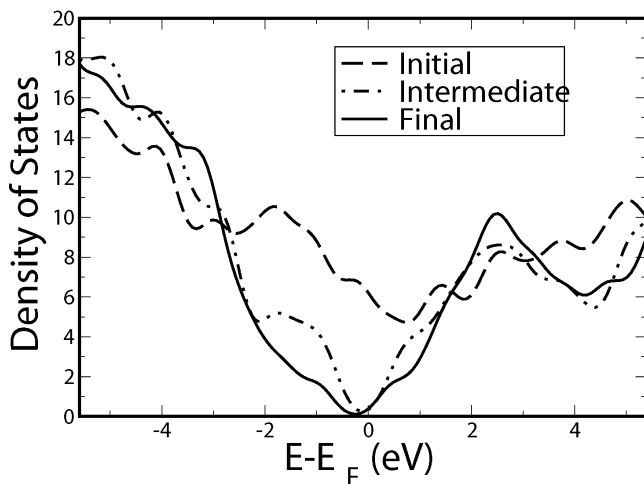


Figure 5. Evolution of the total density of states,  $D(E)$ , of a B–C–N layer built from sample c, which has an equal number of B, C, and N atoms, on three stages of the simulated annealing process. The position of the B, C, and N atoms in the layer unit cell is shown in the top panel of Figure 1 for the three stages.

Another interesting feature of the band structure of the B–C–N nanotube in the final stage, seen in Figure 5, is that the two uppermost valence bands and the two lowest conduction bands (in the vicinity of  $E_F$ ) are sparse (*i.e.*, well-separated in energy) and dispersionless (*i.e.*, they are flat bands). Our interpretation for the origin of those flat bands is that they are essentially electronic states confined to the graphene “island” that is immersed in the BN matrix. These states, similarly to those in ordered C/BN nanotubes,<sup>23</sup> decay exponentially away from the graphene island, and as the islands are relatively distant from each other, the hopping matrix element  $t$  between islands is rather small. As bandwidths scale as  $t$ , this leads to bands with very small dispersion. These states will not contribute to electronic transport, and their energies will be in the mobility gap region of

this disordered material. Therefore, the single-particle band gap and the mobility gap may differ significantly.

The confinement of electronic states near  $E_F$  at the graphene islands of the B–C–N nanotube in the final stage of the simulated annealing process, discussed in the preceding paragraph, also occurs in the B–C–N layer. This can be seen in Figure 8, which shows the partial density of states (PDOS) projected at B, C, and N atoms of the B–C–N layer built from sample c at the final stage of the simulated annealing process. The B-projected and the N-projected PDOS are strongly depleted in a wide energy region (of about 4–5 eV) near  $E_F$ . This is characteristic of the electronic structure of the BN layer, which has a wide band gap. In contrast, the C-projected PDOS is much less depleted near  $E_F$ , depicting the “V shape” of graphene. Therefore, the electronic states with energies between –7 and –2 eV will be

essentially electronic states confined to the graphene island.

We have investigated so far the electronic structure of sample c, which has the same number (32) of B, C, and N atoms. What would be the effect of deviations from this stoichiometry on the electronic structure? To investigate that, we calculated the (broadened) density of states  $D(E)$  for samples e, f, and g, which have stoichiometries that differ from that of sample c at their final, converged, atomic configurations. These  $D(E)$  values are shown in Figures 8, 9, and 10. The figures also show, as vertical dashed lines, the energy values corresponding to the highest occupied molecular orbital (HOMO) and the lowest unoccupied molecular orbital (LUMO) eigenvalues. The HOMO and LUMO eigenvalues of all samples in their final configurations are also listed in Table 1.

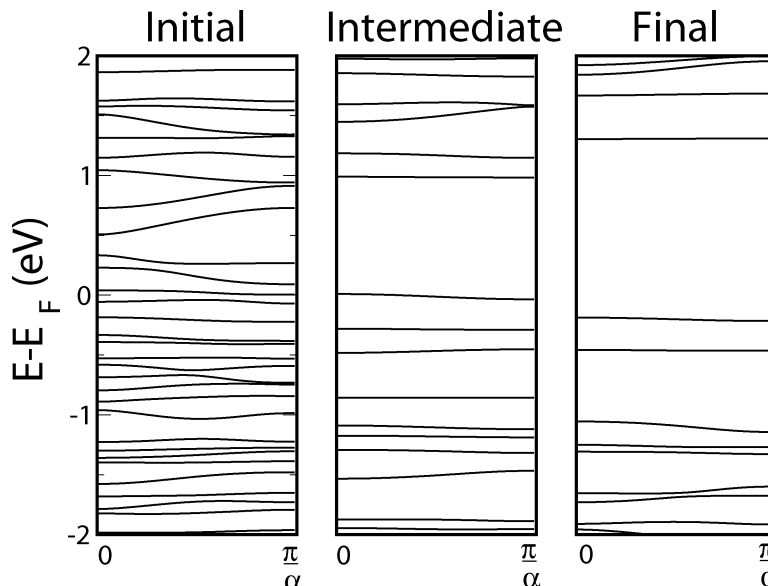


Figure 6. Evolution of the band structure of the (4,4) B–C–N nanotube built from sample c at three stages of the simulated annealing. The position of the B, C, and N atoms in the nanotube unit cell is shown in the bottom panel of Figure 1 for the three stages.

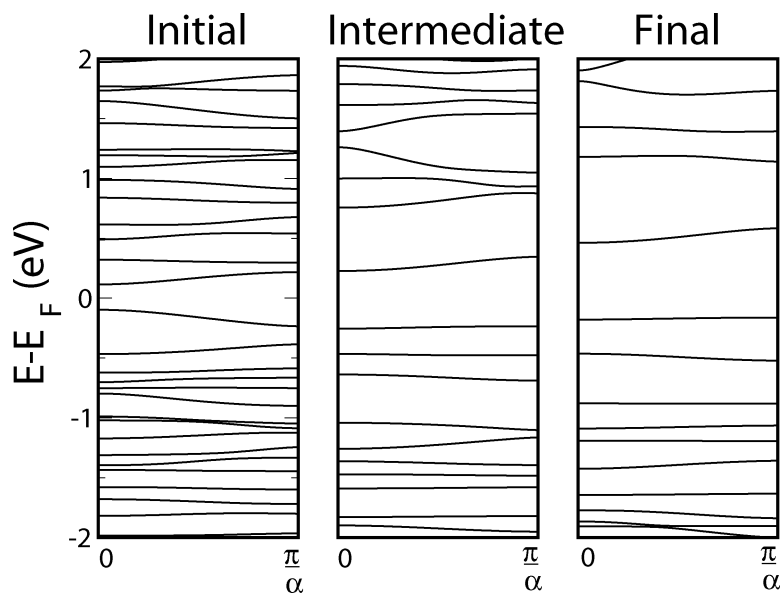


Figure 7. Evolution of the band structure of the (6,0) B–C–N nanotube built from sample c at three stages of the simulated annealing. The position of the B, C, and N atoms in the nanotube unit cell is shown in Figure 2 for the three stages.

Figure 9 shows the density of states (DOS) for sample e, which has the same number of B and N at-

oms (34), but which has a smaller carbon content as compared to sample c. A comparison between Figures 8 (for sample e) and 7 (for sample c) shows that the electronic structure is very similar for both cases, except that, for sample e, the projected  $D(E)$  at the carbon atoms has a smaller weight, as expected. This suggests that small variations in carbon content would lead to small modifications in electronic properties.

Figure 10 shows  $D(E)$  for sample f, which has more B atoms (34) than N atoms (31). By comparing this result with that of the (stoichiometric) sample c, shown in Figure 7, one can see the following major modifications: (i) the appearance of a new peak in  $D(E)$  at  $E_F$ , near the energy value of the top of the valence band of the stoichiometric sample c; (ii) the HOMO and the LUMO are near each other and right at the center of the new peak in  $D(E)$ . Our interpretation is that this new peak has the characteristics of an acceptor impurity band, which is consistent with the excess of (acceptor-type) B atoms. The reason for the small band gap, in this case, is the fact that  $E_F$  lies at the center of an energy region with a high density of states.

Figure 11 shows  $D(E)$  for sample g, which has more N atoms (34) than B atoms (31). By comparing this  $D(E)$  with that of the (stoichiometric) sample c, shown in Figure 7, one can see the following major modifications: (i) similar to the previous case (sample f), there is a new peak in  $D(E)$  at  $E_F$ , but in the present case, it is near the energy value of the bottom of the conduction band of the stoichiometric sample c; (ii) the HOMO and the LUMO are near each other, and right at the center of the new peak in  $D(E)$ . Our interpretation is that this new peak has the characteristics of a donor impurity band, which is consistent with the excess of (donor-type) N atoms. The reason for the small band gap, similar to the previous case, is the fact that  $E_F$  lies at the center of an energy region with a high density of states.

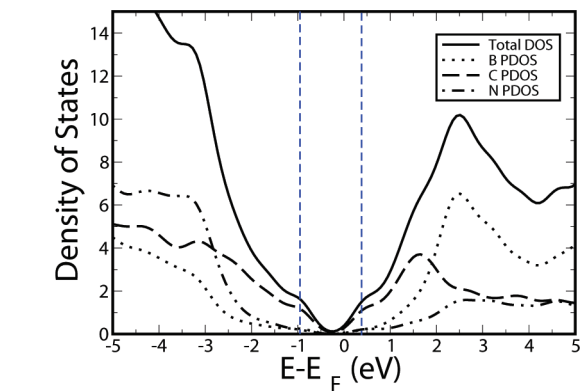


Figure 8. Partial density of states projected at B, C, and N atoms of the B–C–N layer built from sample c at the final stage of the simulated annealing process. The vertical dashed lines indicate the HOMO and the LUMO eigenvalues.

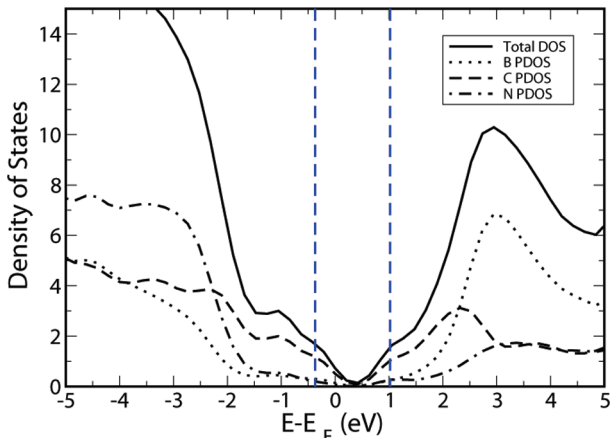


Figure 9. Partial density of states projected at B, C, and N atoms of the B–C–N layer built from sample e at the final stage of the simulated annealing process. The vertical dashed lines indicate the HOMO and the LUMO eigenvalues.

The appearance of features in  $D(E)$  resembling acceptor or donor impurity bands in the case of samples with excess of B or N atoms, respectively, as well as the featureless behavior of  $D(E)$  near  $E_F$  in the initial, random configurations might be related to the nature of the on-site disorder in the Hamiltonian of B–C–N systems. Many years ago, Velicky *et al.*<sup>37,38</sup> investigated the properties of a disordered binary alloy within a tight-binding-type Hamiltonian. The main parameters of that model were the on-site disorder  $\delta = (E_A - E_B)/w$ , where  $E_A$  and  $E_B$  are the on-site matrix elements at sites of atom type A and B, respectively, and  $w$  is the valence bandwidth; and  $c$ , the relative concentration of type A atoms. One of their results was that the virtual crystal approximation (VCA)<sup>38</sup> is only applicable for small values of  $\delta$ ; in that case, the band structure of the mixed alloy resembles that of a pure A or B system. For this reason, the small  $\delta$  regime was named VCA regime.<sup>38</sup> For larger values of  $\delta$ , the VCA is not a good approximation, and the electronic structure of the disordered system is in the so-called regime of split-off impurity band,<sup>38</sup> so named because an impurity band is formed above the host band for small values of  $c$ . We have observed three independent features that suggest that the B–C–N system is in the regime of split-off impurity band. First, the difference  $E_N - E_B$  between the on-site matrix elements of the boron and the nitrogen sites is of the order of 5 eV (in a nearest-neighbor hopping orthogonal basis tight-binding model, the band gap of BN is given by  $E_N - E_B$ ). Therefore,  $\delta$  is not small. Second, the DOS for systems with a small excess of B or N atoms (see Figures 9 and 10) depicts features that resemble split-off bands (near the top of the valence band for B excess and near the bottom of the conduction band for N excess). Third, the VCA would lead to a qualitatively incorrect result if applied to this system in the initial, disordered configuration, for the following reason: within VCA, the Hamiltonian would be that of a “renormalized graphene”, and the resulting DOS would have the same qualitative feature as that of graphene, that is, null at  $E_F$  and V-shaped in the vicinity of  $E_F$ . This is qualitatively different from our first-principles result for the initial, disordered configuration, which is a finite and featureless  $D(E)$  near  $E_F$ .

## CONCLUSIONS

In the present work, we investigated structural and electronic properties B–C–N layers and nanotubes considering the positional disorder of the B, C, and N atoms, with a combination of *ab initio* and empirical

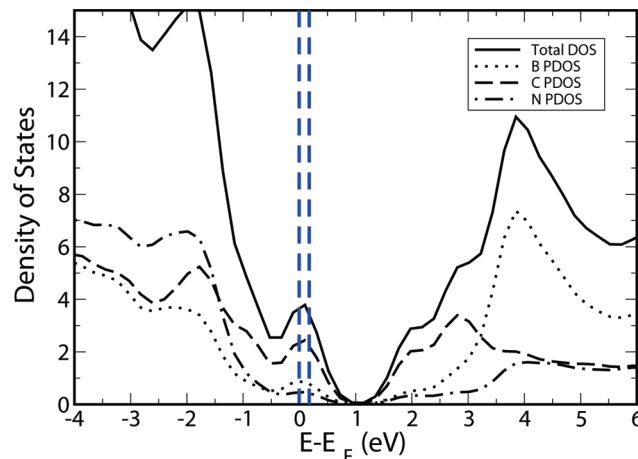


Figure 10. Partial density of states projected at B, C, and N atoms of the B–C–N layer built from sample f at the final stage of the simulated annealing process. The vertical dashed lines indicate the HOMO and the LUMO eigenvalues.

model calculations. During the annealing process, we find that the carbon atoms segregate into isolated islands immersed in the BN layer. In the case of layers and nanotubes with the same number of B and N atoms, we find that the band gap increases during the simulated annealing. This indicates that, for a given stoichiometry, the electronic and optical properties of B–C–N layers and nanotubes can be tuned by growth kinetics. We also find that small deviations from the ideal 1:1:1 stoichiometry may lead to large variations in the band gap and work function.

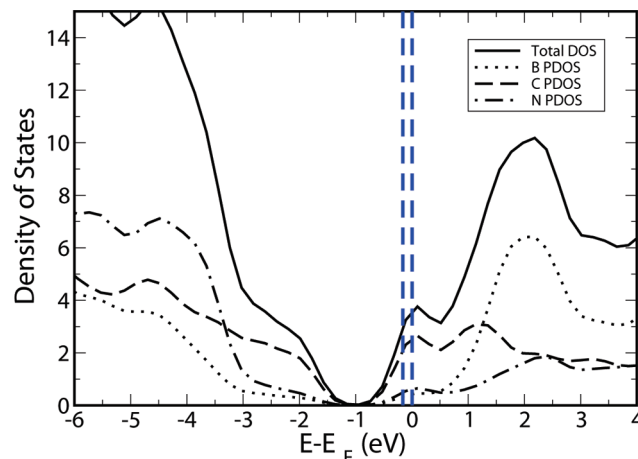


Figure 11. Partial density of states projected at B, C, and N atoms of the B–C–N layer built from sample g at the final stage of the simulated annealing process. The vertical dashed lines indicate the HOMO and the LUMO eigenvalues.

## METHODS

The total energies used in the simulated annealing procedure are calculated with the bond-energy model of Mazzoni *et al.*<sup>19</sup> In this model, the total energy is given by

$$E_{\text{model}}^i = \sum_{\alpha\beta} n_{\alpha\beta}^i \epsilon_{\alpha\beta}^i \quad (1)$$

where  $i$  is the structure index,  $\alpha, \beta = C, B, N$ , and  $n_{\alpha\beta}^i$  is the number of  $\alpha, \beta$  bonds in structure  $i$ . The relevant parameters in the model, parametrized from first-principles calculations,<sup>19</sup> are all the possible first-neighbor bond energies, namely,  $\epsilon_{CB}$ ,  $\epsilon_{CN}$ ,  $\epsilon_{BN}$ ,  $\epsilon_{CC}$ ,  $\epsilon_{BB}$ ,  $\epsilon_{NN}$ . In a previous study,<sup>19</sup> it was shown that the bond-energy model of eq 1 allows quantitative predictions as compared to first-principles calculations for small-unit-cell B–C–N structures.

The electronic structure, the energetics, and the geometry of selected configurations obtained in the simulated annealing procedure are investigated from first principles. The first-principles calculations are performed in the framework of Kohn–Sham density functional theory (DFT),<sup>39</sup> within the generalized-gradient approximation (GGA)<sup>40</sup> and norm-conserving pseudopotentials<sup>41</sup> in the Kleinman–Bylander factorized form.<sup>42</sup> We use the LCAO method implemented in the SiESTA code,<sup>43–45</sup> with a double- $\zeta$  basis set plus polarization orbitals. All geometries were relaxed until the total force on each atom was less than 0.05 eV/Å. The calculational parameters are the same as those of a previous work.<sup>19</sup> Similarly to that work, we also find a quantitative agreement between the bond-energy model of eq 1 and the first-principles results: considering the seven theoretical samples in Table 1, the rms deviation between the model energies and the total energies of the first-principles calculations is 9.8 meV/atom, and the largest single deviation is 14 meV/atom (for sample g).

**Acknowledgment.** We acknowledge support from the Brazilian agencies CNPq, FAPEMIG, and from the projects Instituto do Milenio em Nanotecnologia-MCT and Rede Nacional de Pesquisa em Nanotubos de Carbono.

## REFERENCES AND NOTES

- Krivanek, O. L.; Chisholm, M. F.; Nicolosi, V.; Pennycook, T. J.; Corbin, G. J.; Dellby, N.; Murfitt, M. F.; Own, C. S.; Szilagyi, Z. S.; Oxley, M. P.; et al. Atom-by-Atom Structural and Chemical Analysis by Annular Dark-Field Electron Microscopy. *Nature* **2010**, *464*, 571–574.
- Ci, L.; Song, L.; Jin, C.; Jariwala, D.; Wu, D.; Li, Y.; Srivastava, A.; Wang, Z. F.; Storr, K.; Balicas, L.; et al. Atomic Layers of Hybridized Boron Nitride and Graphene Domains. *Nat. Mater.* **2010**, *9*, 430–435.
- Wang, B.; Ma, Y.; Wu, Y.; Li, N.; Huang, Y.; Chen, Y. Direct and Large Scale Electric Arc Discharge Synthesis of Boron and Nitrogen Doped Single-Walled Carbon Nanotubes and Their Electronic Properties. *Carbon* **2009**, *47*, 2112–2115.
- Liao, L.; Liu, K.; Wang, W.; Bai, X.; Wang, E.; Liu, Y.; Li, J.; Liu, C. Multiwall Boron Carbonitride/Carbon Nanotube Junction and Its Rectification Behavior. *J. Am. Chem. Soc.* **2007**, *129*, 9562–9563.
- Yin, L.-W.; Bando, Y.; Golberg, D.; Gloter, A.; Li, M.-S.; Yuan, X.; Sekiguchi, T. Porous BCN Nanotubular Fibers: Growth and Spatially Resolved Cathodoluminescence. *J. Am. Chem. Soc.* **2005**, *127*, 16354–16355.
- Wang, W. L.; Bai, X. D.; Liu, K. H.; Xu, Z.; Golberg, D.; Bando, Y.; Wang, E. G. Direct Synthesis of B–C–N Single-Walled Nanotubes by Bias-Assisted Hot Filament Chemical Vapor Deposition. *J. Am. Chem. Soc.* **2006**, *128*, 6530–6531.
- Kim, S. Y.; Park, J.; Choi, H. C.; Ahn, J. P.; Hou, J. Q.; Kang, H. S. X-ray Photoelectron Spectroscopy and First Principles Calculation of BCN Nanotubes. *J. Am. Chem. Soc.* **2007**, *129*, 1705–1716.
- Li, L. J.; Glerup, M.; Khlobystov, A. N.; Wiltshire, J. G.; Sauvajol, J.-L.; Taylor, R. A.; Nicholas, R. J. The Effects of Nitrogen and Boron Doping on the Optical Emission and Diameters of Single-Walled Carbon Nanotubes. *Carbon* **2006**, *44*, 2752–2757.
- Raidongia, K.; Nag, A.; Hembram, K. P. S. S.; Waghmare, U. V.; Datta, R.; Rao, C. N. R. BCN: A Graphene Analogue with Remarkable Adsorptive Properties. *Chem.—Eur. J.* **2010**, *16*, 149–157.
- Panchakarla, L. S.; Subrahmanyam, K. S.; Saha, S. K.; Govindaraj, A.; Krishnamurthy, H. R.; Waghmare, U. V.; Rao, C. N. R. Synthesis, Structure, and Properties of Boron- and Nitrogen-Doped Graphene. *Adv. Mater.* **2010**, *21*, 4726–4730.
- Stephan, O.; Ajayan, P. M.; Colliex, C.; Redlich, P. H.; Lambert, J. M.; Bernier, P.; Lefin, P. Doping Graphitic and Carbon Nanotube Structures with Boron and Nitrogen. *Science* **1994**, *266*, 1683–1685.
- Weng-Sieh, Z.; Cherrey, K.; Chopra, N. G.; Blase, X.; Miyamoto, Y.; Rubio, A.; Cohen, M. L.; Louie, S. G.; Zettl, A.; Gronsky, R. Synthesis of  $B_xC_yN_z$  Nanotubules. *Phys. Rev. B* **1995**, *51*, 11229–11232.
- Terrones, M.; Grobert, N.; Terrones, H. Synthetic Routes to Nanoscale  $B_xC_yN_z$  Architectures. *Carbon* **2002**, *40*, 1665–1684.
- Bai, X. D.; Wang, E. G.; Yu, J.; Yang, H. Blue-Violet Photoluminescence from Large-Scale Highly Aligned Boron Carbonitride Nanofibers. *Appl. Phys. Lett.* **2000**, *77*, 67–69.
- Blase, X.; Chacham, H. Electronic Properties of Boron-Nitride and Boron Carbonitride Nanotubes and Related Heterojunctions. In *B–C–N Nanotubes and Related Structures*; Yap, Y. K., Ed.; Springer: New York, 2009; pp 83–103.
- Arenal, R.; Blase, X.; Loiseau, A. Boron–Nitride and Boron–Carbonitride Nanotubes: Synthesis, Characterization and Theory. *Adv. Phys.* **2010**, *59*, 101–179.
- Watanabe, M. O.; Itoh, S.; Sasaki, T.; Mizushima, K. Visible-Light-Emitting Layered  $BC_2N$  Semiconductor. *Phys. Rev. Lett.* **1996**, *77*, 187–189.
- Chen, Y.; Barnard, J. C.; Palmer, R. E.; Watanabe, M. O.; Sasaki, T. Indirect Band Gap of Light-Emitting  $BC_2N$ . *Phys. Rev. Lett.* **1999**, *83*, 2406–2408.
- Mazzoni, M. S. C.; Nunes, R. W.; Azevedo, S.; Chacham, H. Electronic Structure and Energetics of  $B_xC_yN_z$  Layered Structures. *Phys. Rev. B* **2006**, *73*, 073108.
- Liu, A. Y.; Wentzcovitch, R. M.; Cohen, M. L. Atomic Arrangement and Electronic Structure of  $BC_2N$ . *Phys. Rev. B* **1989**, *39*, 1760.
- Miyamoto, Y.; Rubio, A.; Cohen, M. L.; Louie, S. G. Chiral Tubules of Hexagonal  $BC_2N$ . *Phys. Rev. B* **1994**, *50*, 4976–4979.
- Blase, X.; Charlier, J. C.; Vita, A. D.; Car, R. Structural and Electronic Properties of Composite  $B_xC_yN_z$  Nanotubes and Heterojunctions. *Appl. Phys. A: Mater. Sci. Process.* **1999**, *68*, 293–300.
- Blase, X.; Charlier, J. C.; Vita, A. D.; Car, R. Theory of Composite  $B_xC_yN_z$  Nanotubes Heterojunctions. *Appl. Phys. Lett.* **1997**, *70*, 197–199.
- Nozaki, H.; Itoh, S. Structural Stability of  $BC_2N$ . *J. Phys. Chem. Solids* **1996**, *57*, 41–49.
- Enyashin, A. N.; Makurin, Y. N.; Ivanovskii, A. L. Quantum Chemical Study of the Electronic Structure of New Nanotubular Systems:  $\alpha$ -Graphyne-like Carbon, Boron–Nitrogen and Boron–Carbon–Nitrogen Nanotubes. *Carbon* **2004**, *42*, 2081–2089.
- Azevedo, S.; Mazzoni, M. S. C.; Nunes, R. W.; Chacham, H. Stability of Antiphase Line Defects in Nanometer-Sized Boron Nitride Cones. *Phys. Rev. B* **2004**, *70*, 205412.
- Dutta, S.; Pati, S. K. Novel Properties of Graphene Nanoribbons: a Review. *J. Mater. Chem.* **2010**, *20*, 8207–8223.
- Kan, E.; Li, Z.; Yang, J.; Hou, J. G. Half-Metallicity in Edge-Modified Zigzag Graphene Nanoribbons. *J. Am. Chem. Soc.* **2008**, *130*, 4224–4225.
- Dutta, S.; Pati, S. K. Half-Metallicity in Undoped and Boron Doped Graphene Nanoribbons in the Presence of Semilocal Exchange–Correlation Interactions. *J. Phys. Chem. B* **2008**, *112*, 1333–1335.
- Datta, S. S.; Strachan, D. R.; Khamis, S. M.; Johnson, A. T. C. Crystallographic Etching of Few-Layer Graphene. *Nano Lett.* **2008**, *8*, 1912–1915.
- Hod, O.; Barone, V.; Peralta, J. E.; Scuseria, G. E. *Nano Lett.* **2008**, *7*, 2295–2299.
- Dutta, S.; Manna, A. K.; Pati, S. K. Intrinsic Half-Metallicity in Modified Graphene Nanoribbons. *Phys. Rev. Lett.* **2009**, *102*, 096601.
- Dutta, S.; Lakshmi, S.; Pati, S. K. Electron–Electron Interactions on the Edge States of Graphene: A Many-Body Configuration Interaction Study. *Phys. Rev. B* **2008**, *77*, 073412.
- Hamada, N. H.; Sawada, S.; Oshiyama, A. New One Dimensional Conductors: Graphitic Microtubules. *Phys. Rev. Lett.* **1992**, *68*, 1579–1581.

35. Blase, X.; Rubio, A.; Cohen, M. L.; Louie, S. G. Stability and Band Gap Constancy of Boron Nitride Nanotubes. *Europhys. Lett.* **1994**, *28*, 335–340.
36. Kirkpatrick, S.; Gelatt, C. D.; Vecchi, M. P. Optimization by Simulated Annealing. *Science* **1983**, *220*, 671–680.
37. Velicky, B.; Kirkpatrick, S.; Ehrenreich, H. Single-Site Approximations in the Electronic Theory of Simple Binary Alloys. *Phys. Rev.* **1968**, *175*, 747–766.
38. Jones, W.; March, N. H. *Theoretical Solid State Physics*; Dover: New York, 1985.
39. Kohn, W.; Sham, L. J. Self-Consistent Equations Including Exchange and Correlation Effects. *Phys. Rev.* **1965**, *140*, A1133–A1138.
40. Perdew, J. P.; Burke, K.; Ernzerhof, M. Generalized Gradient Approximation Made Simple. *Phys. Rev. Lett.* **1996**, *77*, 3865–3868.
41. Troullier, N.; Martins, J. L. Efficient Pseudopotentials for Plane-Wave Calculations. *Phys. Rev. B* **1991**, *43*, 1993–2006.
42. Kleinman, L.; Bylander, D. M. Efficacious Form for Model Pseudopotentials. *Phys. Rev. Lett.* **1982**, *48*, 1425–1428.
43. Gonze, X.; Stumpf, R.; Scheffler, M. Analysis of Separable Potentials. *Phys. Rev. B* **1991**, *44*, 8503–8513.
44. Soler, J. M.; Artacho, E.; Gale, J. D.; García, A.; Junquera, J.; Ordejón, P.; Sánchez-Portal, D. The SIESTA Method for *Ab Initio* Order-N Materials Simulation. *J. Phys.: Condens. Matter* **2002**, *14*, 2745–2779.
45. Ordejón, P.; Soler, J. M.; Artacho, E. Self-Consistent Order-N Density Functional Calculations for Very Large Systems. *Phys. Rev. B* **1996**, *53*, R10441–R10444.
46. Sánchez-Portal, D.; Ordejón, P.; Soler, J. M.; Artacho, E. Density-Functional Method for Very Large Systems with LCAO Basis Set. *Int. J. Quantum Chem.* **1997**, *65*, 453–461.